Electronic band structure and linear optical properties of paraelectric KIO_3

2009 J. Phys.: Condens. Matter 21 125503

(http://iopscience.iop.org/0953-8984/21/12/125503)

J. Phys.: Condens. Matter **21** (2009) 125503 (6pp) doi:10.1088/0953-8984/21/12/125503

Electronic band structure and linear optical properties of paraelectric KIO_3

Bahattin Erdinc[1] **and Harun Akkus**

Physics Department, Yuzuncu Yil University, 65080 Van, Turkey

E-mail: bahattinerdinc@yyu.edu.tr

Received 14 July 2008, in final form 3 December 2008
Published 26 February 2009
Online at stacks.iop.org/JPhysCM/21/125503

Abstract

The electronic energy band structure, partial (PDOS) and total density of states (DOS), and linear optical properties of the paraelectric KIO_3 single crystal are calculated using density functional theory (DFT) in its local density approximation (LDA). The calculated band structure for paraelectric KIO_3 indicates that the crystal has a direct bandgap. Using LDA and generalized gradient approximation (GGA), structural optimization has been performed. The optical spectra of the paraelectric KIO_3 in the photon energy range up to 30 eV are investigated under the scissor approximation. The real and imaginary parts of the frequency-dependent linear dielectric function, as well as related quantities such as energy-loss function, refractive index and effective number of valence electrons, are calculated. The calculated structural optimization and bandgap of the paraelectric KIO_3 have been compared with experimental data and have been found to be in good agreement with the experimental results.

1. Introduction

The materials having the chemical formula ABO_3 have been attractive for extensive investigations due to their interesting electro-optic and electromechanical properties, nonlinearities and fundamental interest in the physics of their phase transitions [1]. The perovskite compounds are on the list of ferroelectrics and they form an important group of these ingenious materials. The perovskite ferroelectric crystals having the chemical formula ABO_3 are the most widely known and investigated ferroelectric materials because of the simplicity of their crystal structures. They are critically important from a technological point of view. A large number of perovskite ABO_3 undergo a series of structural phase transitions ranging from ferroelectric to antiferroelectric with the change in temperature.

Potassium iodate, KIO_3, single crystals have been investigated extensively since 1961 [2, 3]. It transforms from the high temperature pseudocubic paraelectric phase to slightly distorted ferroelectric phases with monoclinic and triclinic structures [2]. KIO_3 is an excellent nonlinear crystal [4, 5] and can be used to fabricate nonlinear optical devices with good optical quality [6]. Therefore, the interest in nonlinear optics has called attention to KIO_3 as a possibly useful nonlinear optical material [7–9]. KIO_3 undergoes successive phase transitions with the temperature change. It has been reported that all phases, except phase I, are ferroelectric at atmospheric pressure. The phase transition temperatures are, respectively, $T_1 = 485$ K (from phase I to phase II), $T_2 = 343$ K (from phase II to phase III), $T_3 = 255/263$ K (on cooling/on heating) (from phase III to phase IV) and $T_4 = 83$ K (from phase IV to phase V) [1]. In the paraelectric phase, phase I, the crystal has a rhombohedral structure with space group $R3m$ ($Z = 1$). In the first ferroelectric phase, phase II, it belongs to the monoclinic class with space group Pm ($Z = 2$). KIO_3 single crystal has a triclinic structure with space group $P1$ ($Z = 4$) in phases III and IV [10]. However, we should emphasize that KIO_3 single-crystal structure has been variously reported as cubic, rhombohedral, monoclinic and triclinic. As far as we know, in all reports to date, there has been no agreement on the phase transitions and on the crystal structures in different phases of KIO_3. Most of these reports have been summarized by Crane [11].

On the other hand, the phase transitions in the KIO_3 have been studied in some detail. Liu *et al* have investigated the phase transition mechanism in KIO_3 single crystals and have calculated the phonon spectra of KIO_3 in rhombohedral phase I, based on DEPT and LDA [10]. Yagi *et al* have investigated the phase transitions using x-ray diffraction and EXAFS measurements to obtain additional structural

[1] Author to whom any correspondence should be addressed.

Table 1. Crystal structure data of paraelectric KIO_3.

			Atom	Wyckoff	x	y	z
Experiment [15]		Space group $R3m$ (160); cell parameter $a = 4.4973$ Å					
		Atomic positions	K	1a	0.511 17	0.511 17	0.511 17
			I	1a	0.000 00	0.000 00	0.000 00
			O	3b	0.028 04	0.028 04	−0.390 94
This work	With only valence electrons	Space group $R3m$ (160); cell parameter $a = 4.5238$ Å					
		Atomic positions	K	1a	0.561 12	0.561 12	0.561 12
			I	1a	0.020 57	0.020 57	0.020 57
			O	3b	−0.021 04	−0.021 04	0.418 59
	With valence plus semicore electrons	Space group $R3m$ (160); cell parameter $a = 4.6571$ Å					
		Atomic positions	K	1a	0.573 34	0.573 34	0.573 34
			I	1a	0.018 65	0.018 65	0.018 65
			O	3b	−0.024 42	−0.024 42	0.415 05

information [12]. Kasatani *et al* have measured the powder x-ray diffraction pattern of KIO_3 in the wide temperature range from 100 to 530 K in order to determine the crystal structure and clarify the mechanism of the successive phase transitions of KIO_3 crystals [13]. Kalinin *et al* performed the structural analysis with single-crystal x-rays [14]. A single-crystal structural analysis for KIO_3 has been said to be difficult by Kasatani *et al*, because of the ferroelectric and ferroelastic complicated domain of the structure [13]. Lucas studied the ferroelectric transition of KIO_3 at the room temperature phase using the neutron powder profile method to resolve the structural uncertainty [15–17]. As far as we know, no *ab initio* general potential calculations of the electronic band structure and optical properties of the ferroelectric phase III of KNO_3 have been reported, in detail.

The space group of rhombohedral KIO_3 belongs to $R3m$, and this crystal is reported to have one molecule in a unit cell and the atomic positions in the unit cell are given in table 1.

In the present work, the paraelectric KIO_3 single crystal has been investigated using the pseudopotential method based on the DFT under the LDA in the rhombohedral phase (phase I). First, the lattice parameters of the rhombohedral KIO_3 crystal have been determined making the volume optimization by the LDA and the GGA using the local experimental crystal structure data [15]. The electronic structure and linear optical properties of the paraelectric KIO_3 have been investigated. The calculated structural optimization and bandgap of the paraelectric KIO_3 are compared with the experimental results.

2. Computational details

The self-consistent norm-conserving pseudopotentials for all atoms of KIO_3 have been generated by using the FHI98PP code [18] with a Troullier–Martins scheme [19]. To investigate the effect of the pseudopotentials generated on the physical properties, especially on the bandgap width, two types of pseudopotential were generated: for only valence electrons, and for valence electrons with semicore electrons. In the first situation, for a potassium atom 4s electron, for iodine atom 5s and 5p electrons and for oxygen atom 2s and 2p electrons; in the second, for potassium atom 3s, 3p and 4s electrons, for iodine atom 4d, 5s, and 5p electrons and for oxygen atom 2s and 2p electrons were considered as the true valence, and the plane waves were used as the basis set for the electronic wavefunctions. Ceperley–Alder Perdew–Wang LDA functional (CAPW-LDA-92) [20] and Perdew–Burke–Ernzerhof GGA functional (PBE-GGA-96) [21] have been used in order to take into account the exchange–correlation effects in the procedure of the generation of pseudopotentials, and in all computations. In order to solve the Kohn–Sham equations [22], the conjugate gradient minimization method [23] was employed by the ABINIT code [24]. All the calculations involve a five-atom rhombohedral unit cell. Good convergence for the bulk total energy calculation has been achieved with the choice of cutoff energies at 45 Hartree using a $6 \times 6 \times 6$ Monkhorst–Pack [25] mesh grid.

As is known, the Kohn–Sham equations determine the ground-state properties. When the optical response calculation is made, thus the self-energy effects must be included. Otherwise the unoccupied conduction bands have no physical significance and a bandgap problem appears: the absorption starts at too low an energy. In order to take into account the self-energy effects, the scissors approximation [26] has been used and the scissor shift, to make the theoretical bandgap match the experimental one, has been chosen at 1 eV in the present work.

It is known that the dielectric function is mainly connected with the electronic response. The dielectric function was calculated in the momentum representation, which requires matrix elements of the momentum $\vec{P}$ between occupied and unoccupied eigenstates. The imaginary part $\varepsilon''(\omega)$ of the dielectric function, $\varepsilon(\omega)$, is given by

$$\varepsilon''(\omega) = \frac{Ve^2}{2\pi\hbar m^2\omega^2} \int \mathrm{d}^3k \sum_{n,n'} |\langle \vec{k}n|\vec{p}|\vec{k}n'\rangle|^2 \times xf(\vec{k}n)(1 - f(\vec{k}n'))\delta(E_{\vec{k}n} - E_{\vec{k}n'} - \hbar\omega), \quad (1)$$

where e is the electron charge, m is the electron mass, V is the volume, $|\vec{k}n\rangle$ is a crystal wavefunction, $\vec{p}$ is the momentum

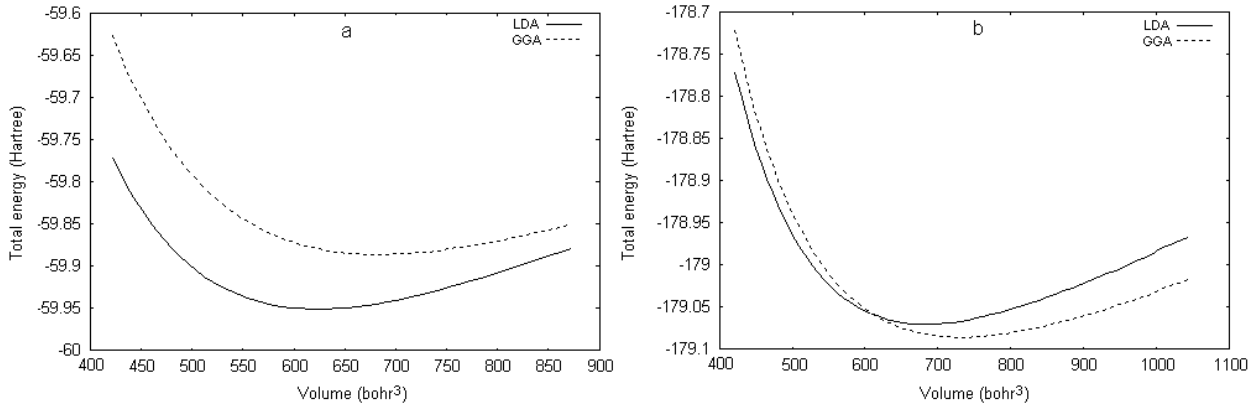

Figure 1. Dependence of total energy on unit cell volume of the rhombohedral KIO_3 single crystal. (a) With only valence electrons and (b) with valence plus semicore electrons.

Table 2. Calculated and experimental lattice parameters, bandgaps and volumes of the rhombohedral KIO_3.

	This work					Deviation (%)			
	With only valence electrons		With valence plus semicore electrons			With only valence electrons		With valence plus semicore electrons	
	GGA	LDA	GGA	LDA	Experiment	GGA	LDA	GGA	LDA
a (Å)	4.6571	4.5238	4.7682	4.6571	4.4973 [15]	3.55	0.59	6.02	3.55
Volume (Å^3)	100.98	92.55	108.37	100.98	90.94 [15]	11.04	1.77	19.16	11.04
Bandgap (eV)	2.25	2.21	2.38	2.31	3–4.5 [1]				

operator, $f(\vec{kn})$ is the Fermi function and $\hbar\omega$ is the energy of the incident photon. The summation over the Brillouin zone is a calculation using a linear interpolation on a mesh of uniformly distributed points. Matrix elements, eigenvalues and eigenvectors are calculated in the irreducible part of the Brillouin zone. The real part $\varepsilon'(\omega)$ of the dielectric function $\varepsilon(\omega)$ is evaluated from the imaginary part $\varepsilon''(\omega)$ by the Kramers–Kronig transformation. All other optical constants of the energy dependence of refractive index $n(\omega)$, energy-loss spectrum $L(\omega)$ and effective number of valence electrons per unit cell, N_{eff}, contributing in the interband transitions by means of the sum rule [27], can be derived from the real part $\varepsilon'(\omega)$ of the dielectric function and the imaginary part $\varepsilon''(\omega)$ of the dielectric function [28].

3. Results and discussion

3.1. Structural optimization

The geometric optimization of the unit cell has been performed for a paraelectric KIO_3 single crystal (phase I) using the crystal structure data determined with the experimental lattice constant ($a = 4.4973$ Å) [15]. All physical properties are related to the total energy. For instance, the equilibrium lattice constant of a crystal is the lattice constant that minimizes the total energy. If the total energy can be calculated, any physical property which is related to the total energy can be determined. The lattice parameter of KIO_3 is also obtained using the pseudopotential method based on the density functional theory under the local density approximation (LDA) and generalized gradient approximation (GGA).

For two cases, both the pseudopotentials with only valence electrons and the pseudopotentials with the valence plus semicore electrons, geometric and atomic optimizations have been performed using both the LDA and GGA separately. The obtained atomic positions are given in table 2. The computed lattice constant by minimizing the ratio of the total energy to the volume for the two cases are given in table 2. The variation of the total energy as a function of the volume is presented in figure 1. As can be seen from table 2 and figure 1, geometric optimization using the LDA is more acceptable than that using the GGA.

3.2. Band structure and density of states

For a better understanding of the electronic and optical properties of KIO_3, the investigation of electronic band structure can be useful. The calculated band structure of paraelectric KIO_3 is shown in figure 2. The band structure has been computed and the high symmetry directions on the surface of the irreducible BZ plotted. The band structure calculations have been performed using two types of pseudopotentials for the ingredient atoms of KIO_3. However, figures 2 and 3 denote only computations in which pseudopotentials with valence plus semicore electrons have been used. It has been seen that the character of the band structure does not change with the choice of pseudopotentials. However, the bandgap width changes with the pseudopotentials used in the band structure calculations. The obtained bandgap values are given in table 2. In figure 2, the Fermi level is set to zero. The bottommost of the

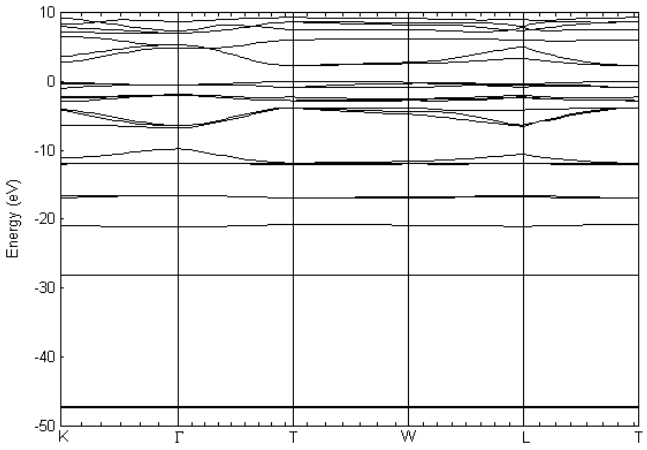

Figure 2. Calculated band structure of the rhombohedral KIO_3 single crystal.

conduction band and the topmost of the valence band are located at the T point (1/2, 1/2, 1/2 in $\boldsymbol{k}$-space) of the BZ. The bandgap values of the crystals like KIO_3 are about 3–4.5 eV [1]. As can be seen from table 2, the calculated bandgap of the paraelectric KIO_3 can be compared with the experimental results. The calculated bandgap is found to be lower than the anticipated 3–4.5 eV range. The origin of this discrepancy may be the LDA which underestimates the bandgaps because of discontinuity in the exchange–correlation potentials which is used in the calculations. The partial density of states (PDOS) and total density of states (DOS) of the paraelectric KIO_3 are investigated. The computed PDOS and DOS are shown in figure 3.

3.3. Optical properties

The optical properties of the paraelectric KIO_3 are shown in figure 4. We have investigated real and imaginary parts of the frequency-dependent linear dielectric function, as well as related quantities such as energy-loss function, refractive index and effective number of valence electrons of the KIO_3 in the energy range up to 30 eV. It is seen that a 0–30 eV photon energy range is sufficient for the optical functions. Thus, we have derived the values of the real and imaginary parts of the dielectric function as a function of the photon energy range up to 30 eV. Since the optical spectra have been analyzed for an energy range 0–30 eV, the spectra contain a lot of peaks which correspond to electronic transitions from the valence band to the conduction band. The values of peaks of the imaginary part of the frequency-dependent dielectric function which are labeled with letters in figure 4 are summarized in table 3. KIO_3 exhibits two fundamental oscillator bands at 4.66 and 6.49 eV, which correspond to the optical transitions from the valence band to the conduction band. Analysis of figure 4 shows that the 0–4.5 eV photon energy range is characterized by high transparency, no absorption and a small reflectivity.

The real part of the frequency-dependent linear dielectric function obtained from the imaginary part by Kramers–Kronig conversion is also presented in figure 3. The calculated static dielectric constant for KIO_3 is 4.01. The dielectric real function is equal to zero at 22.44 and 24.22 eV. The interband transitions at these points, which consist mostly of plasmon excitations, the scattering probability of volume and surface losses are directly connected to the energy-loss function.

The calculated energy-loss functions, $-Im\varepsilon^{-1}$ for volume and $-Im(1+\varepsilon)^{-1}$ for surface, are illustrated in figure 4. The energy-loss functions describe the energy loss of the fast

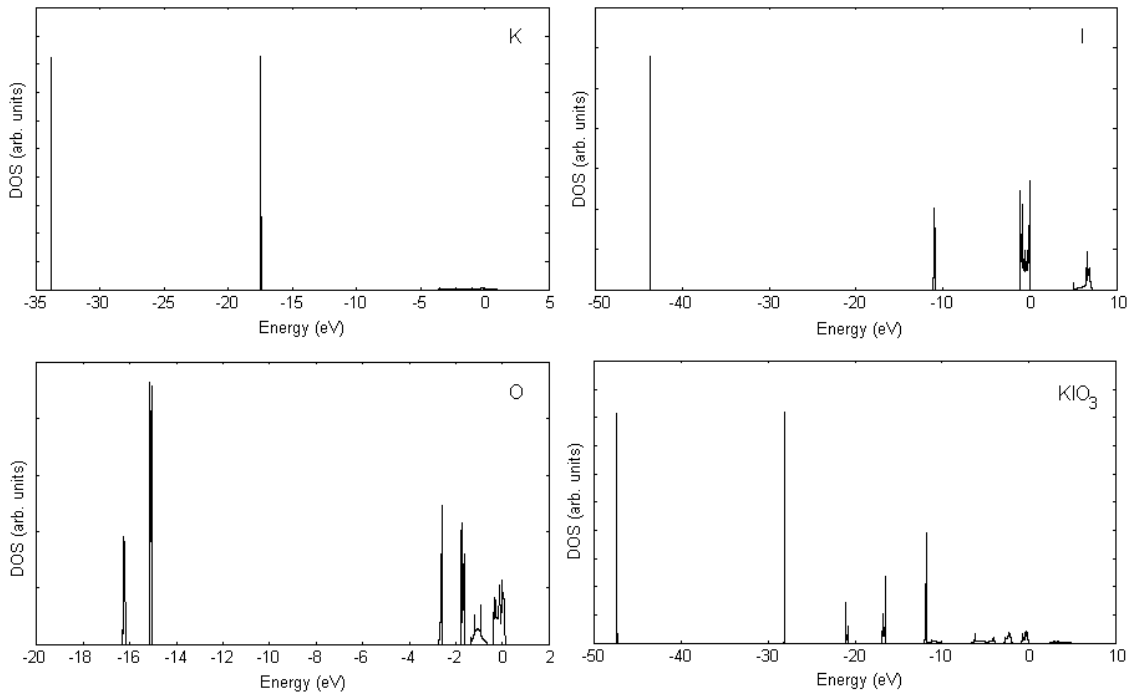

Figure 3. The partial density of states (PDOS) and total density of states (DOS) of the paraelectric KIO_3.

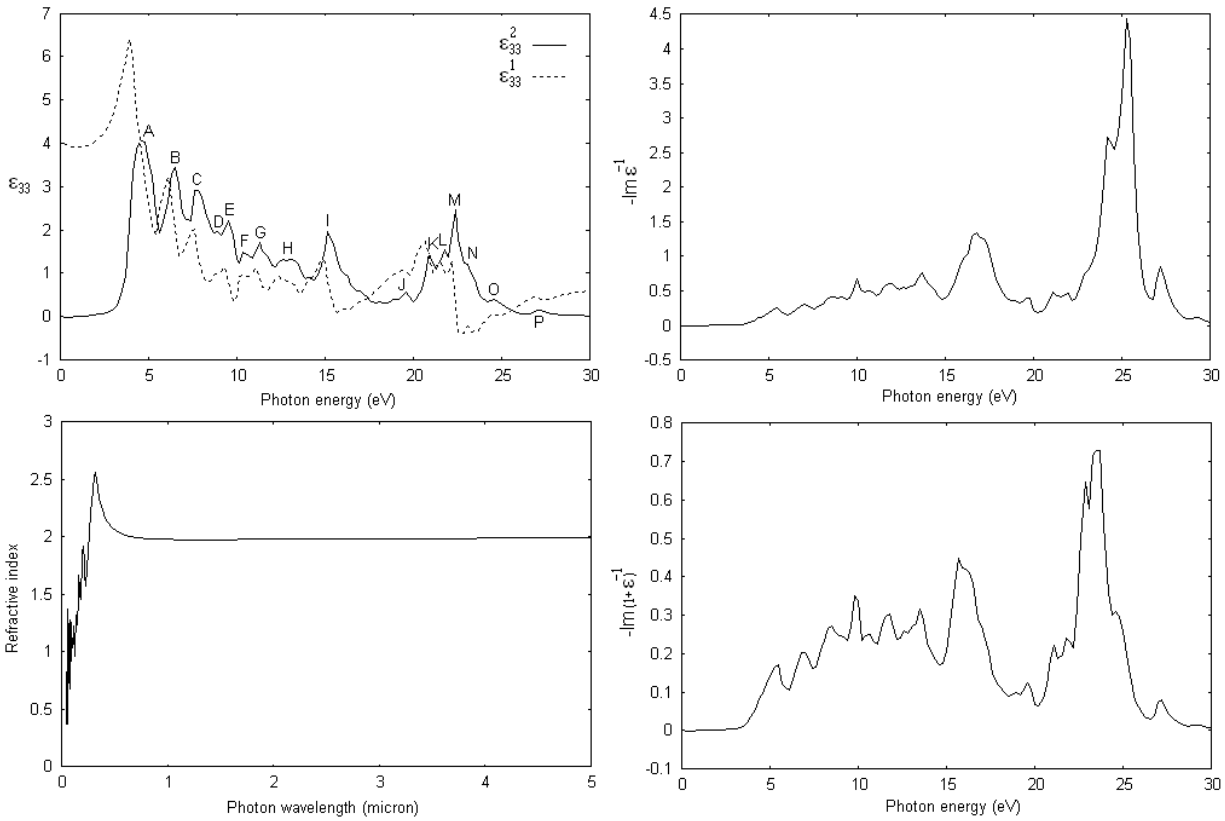

Figure 4. Optical spectra for rhombohedral KIO_3 single crystal.

Table 3. Comparative characteristics of the linear optical functions of the paraelectric KIO_3 single crystal.

	Peaks (eV)															
	A	B	C	D	E	F	G	H	I	J	K	L	M	N	O	P
ε_2	4.66	6.49	7.76	8.89	9.52	10.37	11.28	12.76	15.16	19.53	20.87	21.71	22.35	23.05	24.54	27.07

electrons transversing the material. The sharp maxima in the energy-loss functions are associated with the existence of plasma oscillations. The calculated energy-loss function for volume shows mainly sharp maxima peaks at 16.76 and 25.24 eV. The peak value of volume loss, 25.24 eV, coincides with the zero values of the real part of the dielectric function. The calculated energy-loss function for the surface shows mainly sharp peaks at 15.65 and 23.48 eV. As can be seen from figure 4, the sharp maxima in the energy-loss functions are associated with the existence of plasma oscillations or the energy of the volume and surface plasmon $\hbar\omega_p$.

Figure 4 also presents the spectral dependence of the calculated main refractive index for a paraelectric KIO_3 single crystal in a wide wavelength range. In order to calculate the refractive index, we have chosen a photon wavelength range of 0–5 μm and have seen that a 0–5 μm photon wavelength range is sufficient for the refractive index. It is seen from the figure that the refractive index decreases with the transition from the intrinsic absorption region towards long waves, i.e. a normal dispersion takes place. In the $n = n(\lambda)$ dependence has been obtained a maximum for $\lambda = 0.319$ μm. The maximum value is $n = 2.56$.

We have investigated the effective number of valence electrons of the KIO_3 as a function of the photon energy in the photon energy range up to 30 eV. The effective number of valence electrons per unit cell contributing to the optical constants in the interband transitions can be calculated by means of the sum rule [27]. One can obtain an estimate of the distribution of oscillator strengths for both intraband and interband transitions by computing the $N_{\mathrm{eff}}(E_0)$ defined according to

$$N_{\mathrm{eff}}(E_0) = \frac{2m\varepsilon_0}{\pi\hbar^2 e^2}\frac{1}{N_0}\int_0^{E_0}\varepsilon''(E')E'\,\mathrm{d}E', \qquad (2)$$

where $N_{\mathrm{eff}}(E_0)$ is the effective number of electrons contributing to optical transitions below an energy of E_0. E_0 denotes the upper limit of integration, the quantities m and e are the electron mass and charge, respectively, and N_0 stands for the electron density. As can be seen from figure 5, the effective electron number, $N_{\mathrm{eff}}(E_0)$, up to 3.50 eV is zero, then rises rapidly and reaches a saturation value above 27.50 eV. This shows that the deep-lying valence states do not participate in the interband transition.

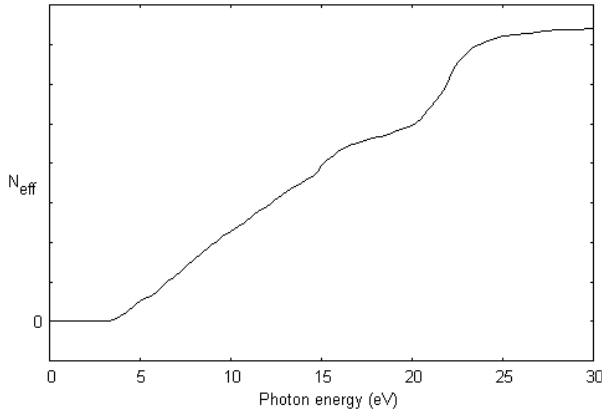

Figure 5. Effective number of valence electrons of the paraelectric KIO_3.

4. Conclusions

As far as we know, the studies concerning KIO_3 are few and most deal with the crystal structure of KIO_3 in the literature. The crystal has a simple structure with five atoms per unit cell. The main object of the present work was to perform a first-principles investigation of paraelectric KIO_3. The results of the implemented structural optimization are in excellent agreement with the experimental results. We have not found any precise reference about the bandgap value of KIO_3 in the literature; however, we know that the bandgap value of crystals like KIO_3 is about 3–4.5 eV. Also, for all we know, any first-principles study about optical properties of KIO_3 does not exist. So, in this paper, we have made a detailed investigation of the electronic structure and optical properties of KIO_3 using the DFT. The partial PDOS and total DOS are obtained from our first-principles calculations. The calculations show that the fundamental gap of KIO_3 is direct. The energy-dependent dielectric constants as well as related quantities such as refractive index, energy-loss function and effective number of valence electrons have been calculated. The results of structural optimization of the paraelectric KIO_3 are in good agreement with the experimental results.

Acknowledgment

This research was supported in part by TUBITAK through the TR-Grid e-Infrastructure Project. See http://www.grid.org.tr for more information.

References

[1] Lines M E and Glass A M 1977 *Principles and Applications of Ferroelectrics and Related Materials* (Oxford: Clarendon)
[2] Herlach F 1961 *Helv. Phys. Acta* **34** 305
[3] Naray-Szabo I and Kalman A 1961 *Acta Crystallogr.* **14** 791
[4] Filimonov A A, Lomova L G, Suvorov V S, Pakhomov V I and Sonin A S 1965 *Kristallografiya* **10** 255
[5] Filimonov A A, Lomova L G, Suvorov V S, Pakhomov V I and Sonin A S 1965 *Sov. Phys.—Crystallogr.* **10** 202
[6] Yin X and Lu M K 1992 *Appl. Phys. Lett.* **60** 2849
[7] Bergman J G, Ashkin A, Boyd G D and Kurtz S K J 1969 *Appl. Phys.* **40** 2860
[8] Guiliani J F and Goldberg L S 1971 *NRL Report 7273*
[9] Kurtz S K and Perry T T J 1968 *Appl. Phys.* **39** 3798
[10] Liu L, Wu R Q, Ni Z H, Shen Z X and Feng Y P 2006 *J. Phys.: Conf. Ser.* **28** 105
[11] Crane G R 1972 *J. Appl. Crystallogr.* **5** 360
[12] Yagi K, Umezawa S, Terauchi H and Kasatani H 2001 *J. Synchrotron. Radiat.* **8** 803
[13] Kasatani H, Aoyagi S, Kuroiwa Y, Yagi K, Katayama R and Terauchi H 2003 *Nucl. Instrum. Methods Phys. Res.* B **199** 49
[14] Kalinin V R, Lylukhin V V and Below N V 1978 *Sov. Phys.—Dokl.* **12** 1978
[15] Byrom P G and Lucas B W 1987 *Acta Crystallogr.* C **43** 1649
[16] Lucas B W 1984 *Acta Crystallogr.* C **40** 1989
[17] Lucas B W 1985 *Acta Crystallogr.* C **41** 1388
[18] Fuchs M and Scheffler M 1999 *Comput. Phys. Commun.* **119** 67
[19] Troullier N and Martins J L 1990 *Phys. Rev.* B **43** 1993
[20] Perdew J P and Wang Y 1992 *Phys. Rev.* B **45** 13244
[21] Perdew J P, Burke K and Ernzerhof M 1996 *Phys. Rev. Lett.* **77** 3865
[22] Kohn W and Sham L J 1965 *Phys. Rev.* **140** A1133
[23] Payne M C, Teter M P, Allan D C, Arias T A and Joannopoulos J D 1992 *Rev. Mod. Phys.* **64** 1045
[24] Gonze X, Beuken J M, Caracas R, Detraux F, Fuchs M, Rignanese G M, Sindic L, Verstrate M, Zerah G, Jollet F, Torrent M, Roy A, Mikami M, Ghosez P, Raty J Y and Allan D C 2002 *Comput. Mater. Sci.* **25** 478
[25] Monkhorst H J and Pack J D 1976 *Phys. Rev.* B **13** 5188
[26] Hughes J L P and Sipe J E 1996 *Phys. Rev.* B **53** 10751
[27] Philipp H R and Ehrenreich H 1963 *Phys. Rev.* **129** 1550
[28] Saha S and Sinha T P 2000 *Phys. Rev.* B **62** 8828